MDPI

*Article*

# Dynamic Mechanics and Crystal Structure Fracture Characteristics of Rock-like Materials in Coal Mines

**Pengfei Gao, Mengxiang Wang \*, Xiaolei Lei and Qi Zong**

School of Civil Engineering and Construction, Anhui University of Science and Technology, Huainan 232001, China; pfgao@aust.edu.cn (P.G.); xllei@aust.edu.cn (X.L.); qzong@aust.edu.cn (Q.Z.)
\* Correspondence: mxwang@aust.edu.cn

**Abstract:** Deep rock bears dynamic loads such as machinery, blasting and disturbance in the mining process. The dynamic fracture mechanism of deep rock is a necessary prerequisite for engineering design and analysis. To study the dynamic fracture mechanism of rock under high in situ stress, deep mudstone and sandstone were selected as research objects. The dynamic mechanical properties and energy dissipation of mudstone sandstone were assessed by using a 50 mm diameter separated Hopkinson test device. According to the similarity criterion, the similarity of strength was assumed as primary factor to prepare similar model materials. Then, dynamic mechanical tests of these similar materials were carried out under dynamic compression splitting and active confining pressure. The results show that materials similar to mudstone and sandstone mainly show axial fracture tensile failure and crushing failure. Both the average strain rate dynamic strength and peak strain of these similar materials increase with increasing impact pressure, and the dynamic strength of similar materials increases exponentially with increasing strain rate. This result is consistent with the regularity of original rock. The dynamic splitting of mudstone-like materials is dominated by the failure of intermediate cracks, and sandstone-like materials also show secondary cracks in addition to intermediate splitting cracks. The dynamic peak strength of mudstone-like materials increases with increasing active confining pressure, and the dynamic peak strength of sandstone-like materials increases nearly twofold under the action of active confining pressure.

**Keywords:** rock-like materials; dynamic compression characteristics; dynamic splitting characteristics; active confining pressure; fracture

## 1. Introduction

The mechanical properties of deep rocks under static or quasi-static loads have been extensively analyzed for decades. Liqinghui et al. [1] carried out experimental research on rock mechanical properties of ultra deep sandstone reservoir, and obtained systematic research on rock mechanical parameters such as uniaxial compression, triaxial compression, Brazil test, shear test and brittleness index of ultra deep sandstone. Zhao [2] analyzed the review of the development of rock mechanics and some unsolved problems for 100 years, and summarized and introduced the rock mechanics testing machine and testing methods. However, affected by mining intensity, coal mines with buried depths of 800–1000, such as Guqiao Coal Mine and Zhangji coal mine, are currently being mined. Deep rocks are inevitably subject to dynamic loads caused by rock burst, collisions, and explosions. The mechanical properties and failure processes of deep rocks under dynamic loads are of great significance [3–5]. In deep rock blasting, rupture, and fragmentation, the energy must be sufficient to break and throw the rocks in the area to be excavated; however, this energy must also be controlled to avoid damage of the retained rock mass by the explosion energy. Deep mudstone and low-strength sandstone have soft rock characteristics, but problems such as difficult rock blasting and low footage during blasting implementation still persist [6–8].

For this reason, deep mudstone and sandstone have been studied to better understand the dynamic mechanical properties and fracture characteristics of sandstone. The main focus of this research was the energy dissipation law of mudstone under dynamic load [9,10]. Compared with static load, the mechanical properties of deep rock under dynamic load change greatly. The size and speed of dynamic load application will affect the mechanical properties of rock. At present, it is generally believed that the dynamic strength of rock increases with the increase in strain rate, and considerable research has been conducted on the topic [10–15]. However, because of the influence of diagenesis, the internal structure of deep coal mine rocks is complex and subject to change. Just as there are no two similar leaves in the world, no two identical rocks can be found in deep coal seams. Rock-like materials can solve this problem. By adjusting the ratio of similar materials, the pouring model of similar materials is matched with a specific key research property of original rock. Then, the law of this key property of such materials under different external loading environments can be studied [16].

To more accurately characterize the material properties of original rock, deep rock samples were subjected to X-ray fluorescence spectroscopy (XRF) and X-ray diffraction (XRD) tests to determine the chemical composition and particle composition of the main components. Based on the dynamic and static mechanical properties of deep rock specimens, and similarity criteria (using similar strength as the primary factor), similar model materials are configured. Dynamic compression, splitting, and impact dynamic mechanical tests of similar materials are carried out under active confining pressure. To simulate the in situ stress of rock as closely as possible, relevant tests were carried out. Informed by the aforementioned analysis of the original rock, similar model materials and similar pouring models were selected to avoid test errors caused by the complexity and unevenness of rock. Simultaneous model tests increase the repeatability of blasting tests.

## 2. Selection of Similar Material Ratio and Static Mechanical Properties

### 2.1. Model Material Ratio Selection

It is often difficult to model materials so that they meet the above-mentioned similarity ratios. To match the similarity conditions as closely as possible, previous test experiences are summarized. It is assumed that geometric dimensions, the matching of explosives and model materials, and the physical and mechanical properties of model materials are key factors affecting similarity. The similarity established by these three factors must be strictly satisfied. Research results both from China and the international community showed that similar model materials are suitable for rock blasting tests. Zuguang and Rustan [17] launched a small-scale experiment on magnetite with similar material models. Bjarnholt [18] obtained similar material properties, and the blasting effect was consistent with medium-strength rock blasting.

The experiment described in this paper used mudstone and sandstone as physical and mechanical properties of the engineering rock mass. Then, the target parameters of the material model were calculated according to the similar material model. The model test was mainly carried out with similar strength or the same strength rock mass. The aim was to simulate the fracture and fracture characteristics of rock masses with different strengths under different confining pressures. When the rock is blasted and broken, the wave impedance ratio should be as similar as possible.

According to the calculation of a similar ratio of mudstone, a material model strength of 18–22 MPa is proposed. Based on the wave impedance similarity coefficient, the mudstone wave impedance ranges from $4.644 \times 10^5$ g/(cm$^2$ s) to $5.676 \times 10^5$ g/(cm$^2$ s) and the density is 2500–2600 kg/m$^3$, the longitudinal wave speed is 1800–2200 m/s, and the similar material is relatively homogeneous. The density is 1900–2000 kg/m$^3$, the longitudinal wave speed is 2850–3000 m/s, and the wave impedance of similar material ranges from $5.4 \times 10^5$ g/(cm$^2$ s ) to $6 \times 10^5$ g/(cm$^2$ s). When configuring materials, a small value should be chosen.

According to the calculation of the similar ratio of sandstone, the material model is proposed to have a strength of 35–42 MPa. Based on the similar coefficient of wave impedance, the wave impedance of mudstone ranges from $8.32 \times 10^5$ g/(cm$^2$ s) to $9.1 \times 10^5$ g/(cm$^2$ s), the density is 2500–2800 kg/m$^3$, and the longitudinal wave speed is 3200–3500 m/s. The similar material is relatively homogeneous, with a density of 2100–2200 kg/m$^3$, a longitudinal wave speed of 3700–3800 m/s, and the wave impedance of similar material ranges from $7.7 \times 10^5$ g/(cm$^2$ s) to $8.36 \times 10^5$ g/(cm$^2$ s). When similar materials are configured, the larger value should be chosen.

In agreement with the test purpose, the test materials for the similarity model of confining pressure loading were based on similar materials. The model materials of similar materials are medium sand, P.C 32.5# composite Portland cement, P.C 42.5# composite Portland cement, tap water, and admixtures. The sand is passed through a 0.2 cm sieve to ensure uniformity of the material. After consulting the data, the building mortar M15 mix ratio was taken as reference. When using 32.5# cement, a proportioning of cement:sand:water:admixture of 1:4:1:0.02 and similar materials for pouring should be used to simulate mudstone. When using 42.5# mud, a proportioning of cement:sand:water:admixture of 2:2:1:0.02 for pouring should be used to simulate sandstone. According to the similar material ratio, when the model is poured, a standard cube test piece is fabricated using a mold of $70 \times 70 \times 70$ mm. Three molds were used per group, and all specimens were vibrated and maintained according to pouring requirements. After the specimens were made, they were cured in saturated calcium hydroxide solution for 28 days. After the model had dried, the volume and mass of standard specimens were measured, and the true density of similar materials was calculated. Although the main components of similar materials of mudstone and sandstone are similar, because the proportions of mixing are different, qualitative and quantitative analysis of similar materials should be conducted. XRF quantitative tests of chemical main components were performed on these two materials, and the results are shown in Table 1.

**Table 1.** Quantitative analysis of X-ray fluorescence spectroscopy (XRF) compositions of rocks and similar materials.

| Chemical Formula | Na$_2$O | MgO | Al$_2$O$_3$ | SiO$_2$ | K$_2$O | CaO | Fe$_2$O$_3$ |
|---|---|---|---|---|---|---|---|
| Mudstone $\omega_B$/% | 1.200 | 1.943 | 20.383 | 56.616 | 3.989 | 0.964 | 12.328 |
| Mudstone-like material $\omega_B$/% | 2.34 | 1.64 | 11.28 | 46.32 | 2.92 | 28.93 | 3.81 |
| Sandstone $\omega_B$/% | 1.91 | 0.944 | 10.910 | 70.63 | 3.386 | 0.81 | 7.011 |
| Sandstone-like materials $\omega_B$/% | 1.68 | 2.02 | 11.539 | 41.414 | 2.91 | 32.87 | 4.53 |

*2.2. Model Material Static Mechanical Test*

The rock mechanics test system (RMT-301) of Anhui University of Science and Technology, China, was used for uniaxial compression tests of specimens. The load was applied at the loading rate of 0.05 KN/s. The measured standard uniaxial compressive strengths of mudstone-like materials and sandstone-like materials are shown in Figure 1.

During the test, the compressive strength results of specimen marked with similar materials were accurate. The strength of mudstone-like material was 16.1 MPa, and the strength of sandstone-like material was 41.8 MPa. However, the measured elastic modulus and Poisson's ratio results show a large error. The reason is that the displacement sensor and initial parameters of the test equipment were not adjusted well during the test. To further test the Poisson's ratio and elastic modulus of similar materials, resistance strain gauges were measured, using resistance strain gauges produced by Zhejiang Huangyan with a 50 AA sensitivity coefficient of 2.0. These are fixed on the surface of the test piece with 502 glue, one horizontally and one vertically. When the specimen is deformed, the resistance of the strain gauge changes. The YE2539 high-speed static strain test system was used to assess the strain value of specimens. The test method refers to the elastic modulus

test method of the concrete specimen. The test process was carried out on a uniaxial rock compression material machine. The location of the test specimen pasting the strain gauge and the test process are shown in Figure 2, and the test data processing result is shown in Figure 3.
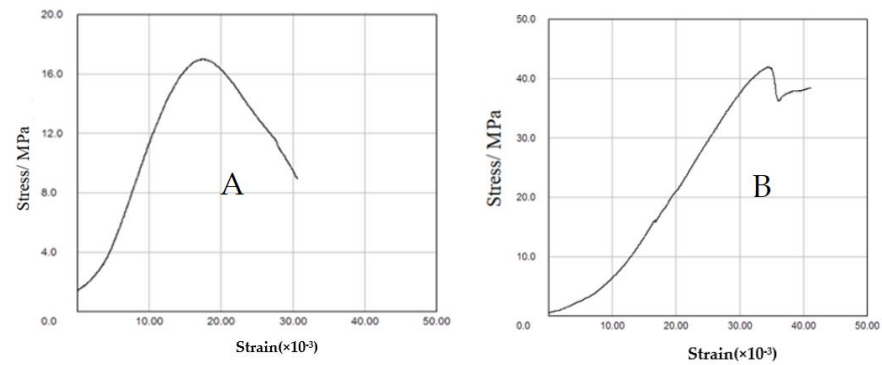


**Figure 1.** RMT−301 test results of similar materials. (**A**) Uniaxial compressive strength of mudstone-like materials; (**B**) uniaxial compressive strength of sandstone-like materials.



**Figure 2.** Static compressive strength and Poisson's ratio of similar materials were tested.

The horizontal and vertical deformations of mudstone-like and sandstone-like materials were tested by pasting strain gauges. Figure 3a shows that the pouring strength of the specimen is consistent with the compressive strength obtained on the RMT, indicating the feasibility of the test data set. Figure 3b shows that the static strain peak of mudstone-like materials exceeds that of sandstone-like materials, and the strain value ranges between 1000 and 2500 microstrains. To calculate the loose ratio, through the linear increase in strain, the corresponding stress section is identified, and the elastic modulus is solved.

The overall shape of static fracture and fracture of sandstone-like materials is shown in Figure 4. The overall shape of failure is similar, mainly representing vertical cracks. The local failure mode of mudstone-like materials is shown in Figure 4a. The main failure mode is exfoliation of the periphery, internal cracks are not apparent, the fragmentation is large, and the typical compressive shear failure occurs in the middle, i.e., the specimen fails at an angle of 45°. Failure appears in the direction and is large at both ends and small in the middle. The local damage pattern of sandstone-like materials is shown in Figure 4b. The overall fragmentation of sandstone exceeds that of mudstone-like materials, and many broken cracks appear on the top. The overall cracks are still mainly vertical, but there are many internal broken areas. In more severe cases, the failure mode of the specimen is trapezoidal compression-shear failure. The reason is that mudstone-like material has a large strain, and there is a compaction stage during the loading process. This makes the contact between the specimen section and the press denser and improves the end friction effect, while sandstone-like material has a small strain value. The material is brittle and

cracks occur in the specimen during the compaction process, i.e., the actual compaction stage is shorter. In the subsequent loading process, the crack area continues to develop, the specimen can withstand the load, and the internal cracks of the material develop rapidly. Dislocation friction emerges and a local broken zone forms.



(a)



(b)
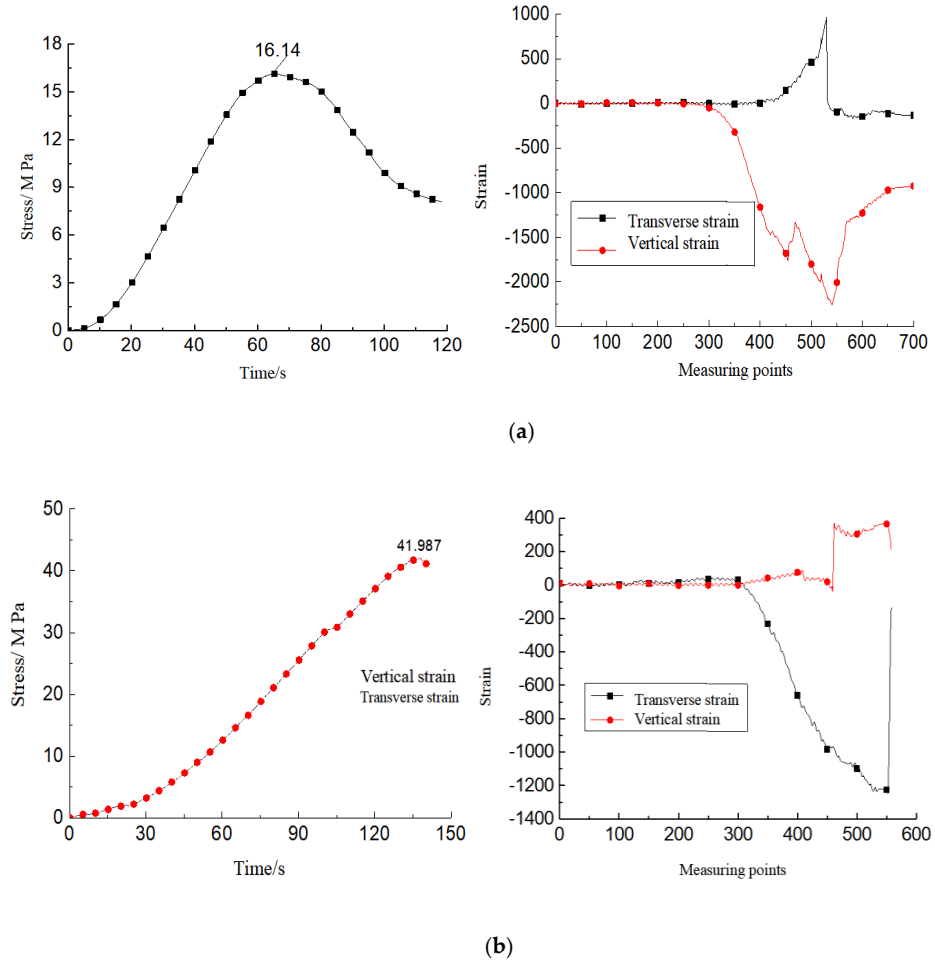
**Figure 3.** Static compressive strength of similar materials is the test result of Poisson's ratio. (**a**) Mudstone-like material test results, (**b**) sandstone-like material test results.



(a)  (b)
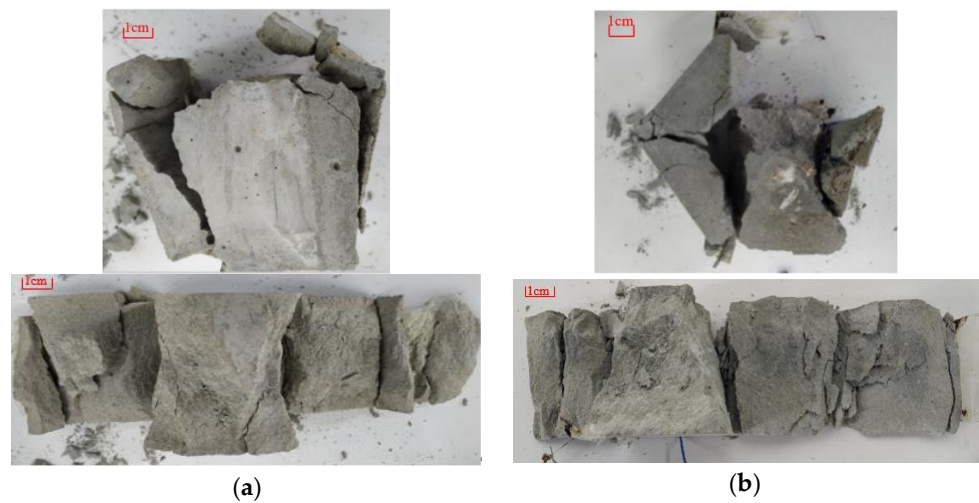
**Figure 4.** Similar material failure modes. (**a**) Internal failure mode of mudstone-like materials, (**b**) internal failure mode of sandstone-like materials.

The physical and mechanical parameters of both similar materials are presented in Table 2. Observation of similar material specimens shows that because of different water-cement ratios and different sand ratios, the sand content of mudstone-like materials is higher, and the specimens appear slightly hairy and yellow, while sandstone-like materials appear blue.

**Table 2.** Physical and mechanical properties of two similar materials.

| Name | True Density (g/cm$^3$) | Longitudinal Wave Velocity (m/s) | Uniaxial Compressive Strength (MPa) | Elastic Modulus (GPa) | Poisson's Ratio (u) |
|---|---|---|---|---|---|
| Mudstone-like material | 1.97 | 2850–2950 | 16.1 | 10 | 0.34 |
| Sandstone-like materials | 2.17 | 3700–3800 | 41.8 | 26 | 0.29 |

## 3. Dynamic Mechanical Properties and Failure Modes of Similar Materials without Confining Pressure

The same the Split Hopkinson pressure bar (SHPB) pressure rod device as mentioned above was adopted, and three driving air pressures of 0.2, 0.3, and 0.4 MPa were used. Six effective data sets on the impact of mudstone-like and sandstone-like materials were obtained. When analyzing the rock fracture characteristics in the SHPB impact test, the forces on both ends of the specimen are a pair of balanced forces. Figure 5 shows a typical stress balance test curve of a test piece, showing that both the processing and placement of the test piece meet the SHPB one-dimensional stress wave hypothesis, end friction, and inertia effect requirements.
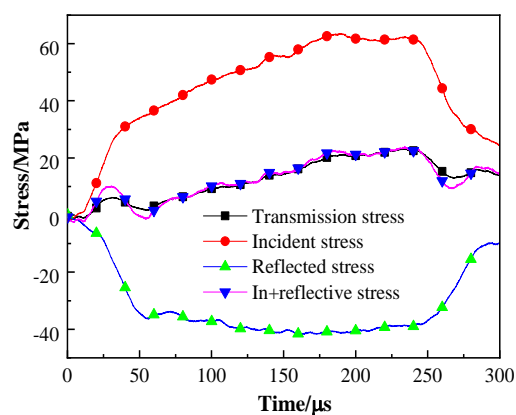


**Figure 5.** Test piece stress balance inspection.

### 3.1. Dynamic Mechanical Analysis of Mudstone-like Materials

Figure 6 shows the typical stress–strain curves of mudstone-like material specimens at different strain rates.

Table 3 shows the average strain rate, dynamic compressive strength, peak strain, and wave impedance of mudstone−like materials under different impact pressures.

The data in Table 3 shows that as the impact pressure increases, the average strain rate of the specimen increases, and the dynamic strength and peak strain of mudstone-like materials also increase. Compared to the static strengths of 0.2, 0.3, and 0.4 MPa, under impact pressure, the dynamic strength of mudstone increased by 1.30, 1.67, and 2.05 times, respectively. The dynamic strength of mudstone-like materials is 1.98, 2.14, and 2.32 times of the static strength, respectively. This shows that similar materials can truly represent mudstone. Figure 6 also shows that the dynamic stress–strain relationship of mudstone-like materials in the test range increases linearly with increasing strain at the initial stage. In the elastic stage, the strain of mudstone does not change significantly but the peak elastic

stress increases. With increasing deformation and when the yield stress is reached, the stress drops sharply, and mudstone-like materials are completely destroyed.
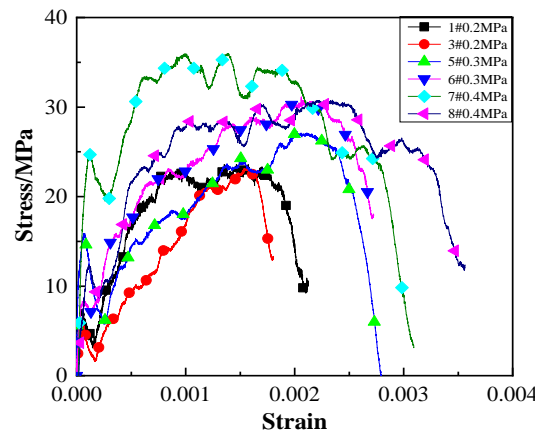


**Figure 6.** Stress–strain curves of mudstone-like samples.

**Table 3.** Experimental data of mudstone-like materials.

| Test Block Number | Impact Air Pressure (MPa) | Specimen Size (Average Value) | | Wave Speed (m/s) | Average Strain Rate $(s^{-1})$ | Peak Stress (MPa) | Peak Strain |
|---|---|---|---|---|---|---|---|
| | | Diameter (mm) | Height (mm) | | | | |
| 1 | 0.2 | 48.91 | 25.78 | 2880 | 81 | 21.15 | 0.0022 |
| 3 | 0.2 | 48.85 | 25.35 | 2801 | 94 | 20.7 | 0.0019 |
| 5 | 0.3 | 48.94 | 25.2 | 2910 | 128 | 25.74 | 0.0030 |
| 6 | 0.3 | 49.11 | 25.00 | 2967 | 130 | 28.12 | 0.0028 |
| 7 | 0.4 | 49.00 | 26.65 | 2840 | 139 | 30.40 | 0.0033 |
| 8 | 0.4 | 49.00 | 24.92 | 2802 | 156 | 35.67 | 0.0037 |

Note: Considering the discrete type of impact test, two relatively close test data sets were selected for each group.

### 3.2. Analysis of Dynamic Mechanical Properties of Sandstone-like Materials

Table 4 shows the average strain rate, dynamic compressive strength, peak strain, and wave impedance of sandstone under different impact pressures. Typical stress–strain curves at different strain rates are shown in Figure 7.

**Table 4.** Sandstone experimental data.

| Test Block Number | Impact Air Pressure (MPa) | Specimen Size (Average Value) | | Wave Speed (m/s) | Average Strain Rate $(s^{-1})$ | Peak Stress (MPa) | Peak Strain $\varepsilon$ |
|---|---|---|---|---|---|---|---|
| | | Diameter (mm) | Height (mm) | | | | |
| 9 | 0.2 | 49.37 | 25.82 | 3596 | 52 | 44.93 | 0.0010 |
| 10 | 0.2 | 49.55 | 25.53 | 3644 | 54 | 47.14 | 0.0011 |
| 11 | 0.3 | 49.37 | 26.10 | 3521 | 77 | 66.15 | 0.0015 |
| 12 | 0.3 | 49.31 | 25.24 | 3583 | 73 | 57.92 | 0.0014 |
| 13 | 0.4 | 49.26 | 25.14 | 3506 | 92 | 72.02 | 0.0019 |
| 14 | 0.4 | 49.23 | 26.36 | 3561 | 93 | 79.37 | 0.0020 |

Note: Considering the discrete type of impact test, two relatively close test data sets are selected for each group.
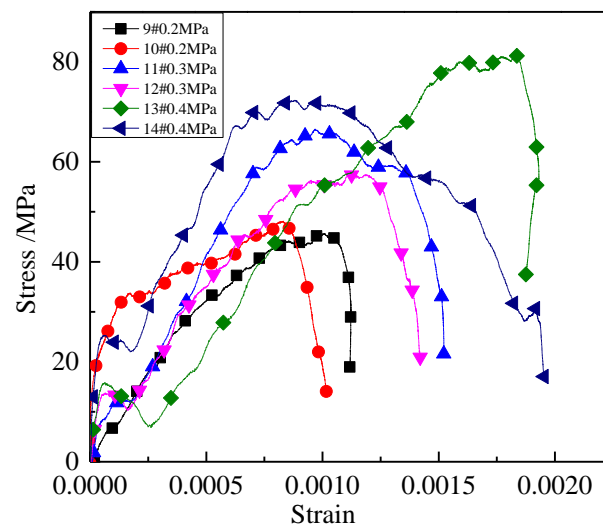
**Figure 7.** Stress–strain curves of sandstone-like materials under different impact pressures.

The data in Table 4 show that with increasing impact pressure, the average strain rate of the specimen is increasing. The average strain rate is smaller than that of mudstone-like materials. Under the same impact pressure, the wave impedance value of sandstone-like materials exceeds that of mudstone-like materials. The reflected wave value of impacting sandstone-like materials is smaller, thereby reducing the strain rate of the material. However, as the static strength of sandstone-like materials exceeds that of mudstone, and the transmission wave increases under consistent impact energy, the dynamic compressive strength of sandstone-like materials far exceeds that of mudstone materials, and the stress growth rate is also greater. The strain of sandstone-like materials is less than that of mudstone-like materials. The reason is that in addition to the higher strength of sandstone-like materials, high cement parameters increase the brittleness of mortar materials, reducing the volumetric strain rate. Figure 7 depicts the dynamic stress–strain relationship of sandstone-like materials within the test range. At the initial stage, stress increases linearly with increasing strain. The peak strain of sandstone-like materials increases significantly with increasing impact pressure. Under the action of impact load, the strain of sandstone-like material is closely related to the impact load, and at this stage, the strain corresponding to the elastic stage of sandstone-like material is greater than that of mudstone-like material. After reaching the elastic limit stress, the dynamic mechanical properties of sandstone-like materials have changed. With increasing deformation, specimens enter the yield deformation stage, but the yield stage is weak. When the yield stress is reached, the stress drops sharply, and samples are completely destroyed.

Figure 8 shows the relationship between dynamic strength and strain rate of similar materials. The dynamic strength of mudstone-like and sandstone-like materials increases according to a power function with increasing strain rate. This is consistent with the regularity of the original rock material, corroborating the feasibility of using these similar materials. The power function exponents of both materials are not very different, but the dynamic strength growth rate of sandstone-like materials under the action of strain rate exceeds that of mudstone-like materials.

### 3.3. Comparison of Macroscopic Damage Patterns of Specimens under Impact

Figure 9 shows the macroscopic failure morphology of mudstone-like and sandstone-like specimens under different impact pressures.

With increasing impact pressure, the fragmentation of specimens of mudstone-like and sandstone-like materials increases, and the size of broken pieces decreases. Under the state of 0.2 MPa, specimen failure shows clear cracking along the specimen axis, which manifests as axial tensile failure and large fragmentation; under the state of 0.3 MPa air pressure

impact, similar mudstone-like specimens are more damaged. The damage of sandstone-like specimens is severe. Mudstone-like materials appear crushed, but the whole specimen is axially fractured and shows tensile failure, and the crushed state appears locally. The sandstone-like specimens have a better broken shape and show large fragmentation; under 0.4 MPa impact pressure, mudstone-like materials are crushed and destroyed. Sandstone-like materials are still broken by axial splitting and tension, but short columnar fragments emerge in the broken state.
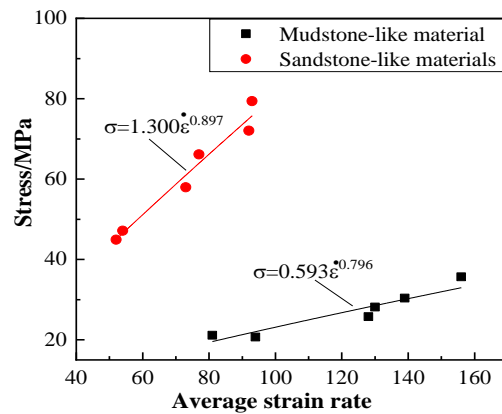


**Figure 8.** Relationship between dynamic strength and strain rate of similar materials.



1 (0.2 MPa broken form)　　　5 (0.3 MPa broken form)　　　8 (0.4 MPa broken form)

(**a**)

3 (0.2 MPa broken form)　　　8 (0.3 MPa broken form)　　　13 (0.4 MPa broken form)

(**b**)
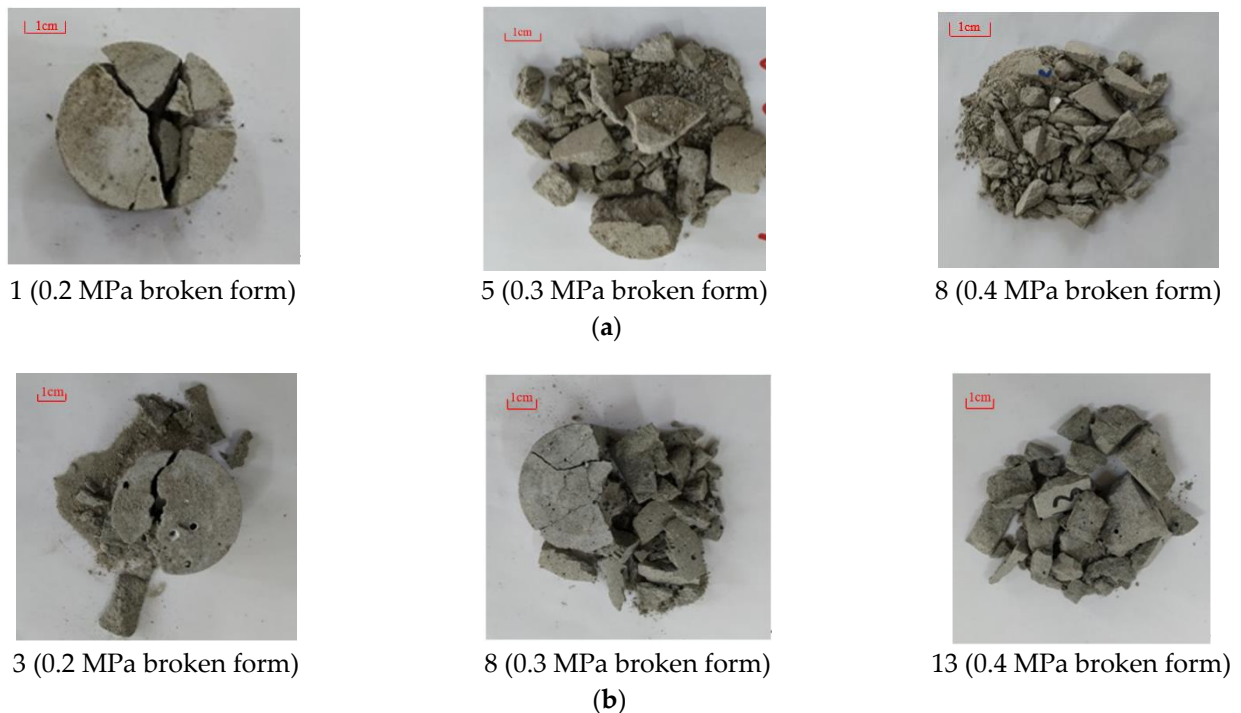
**Figure 9.** Fracture morphology of specimens with different impact pressures. (**a**) Macroscopic impact crushing of mudstone-like materials. (**b**) Macroscopic impact crushing of sandstone-like materials.

### 3.4. Analysis of the Meso-Structural Damage of Specimens

The surface and fracture of mudstone-like and sandstone-like specimens were magnified and observed using the Best Electronic Digital Microscope with a magnification of 1000 times. The results are shown in Figure 10.
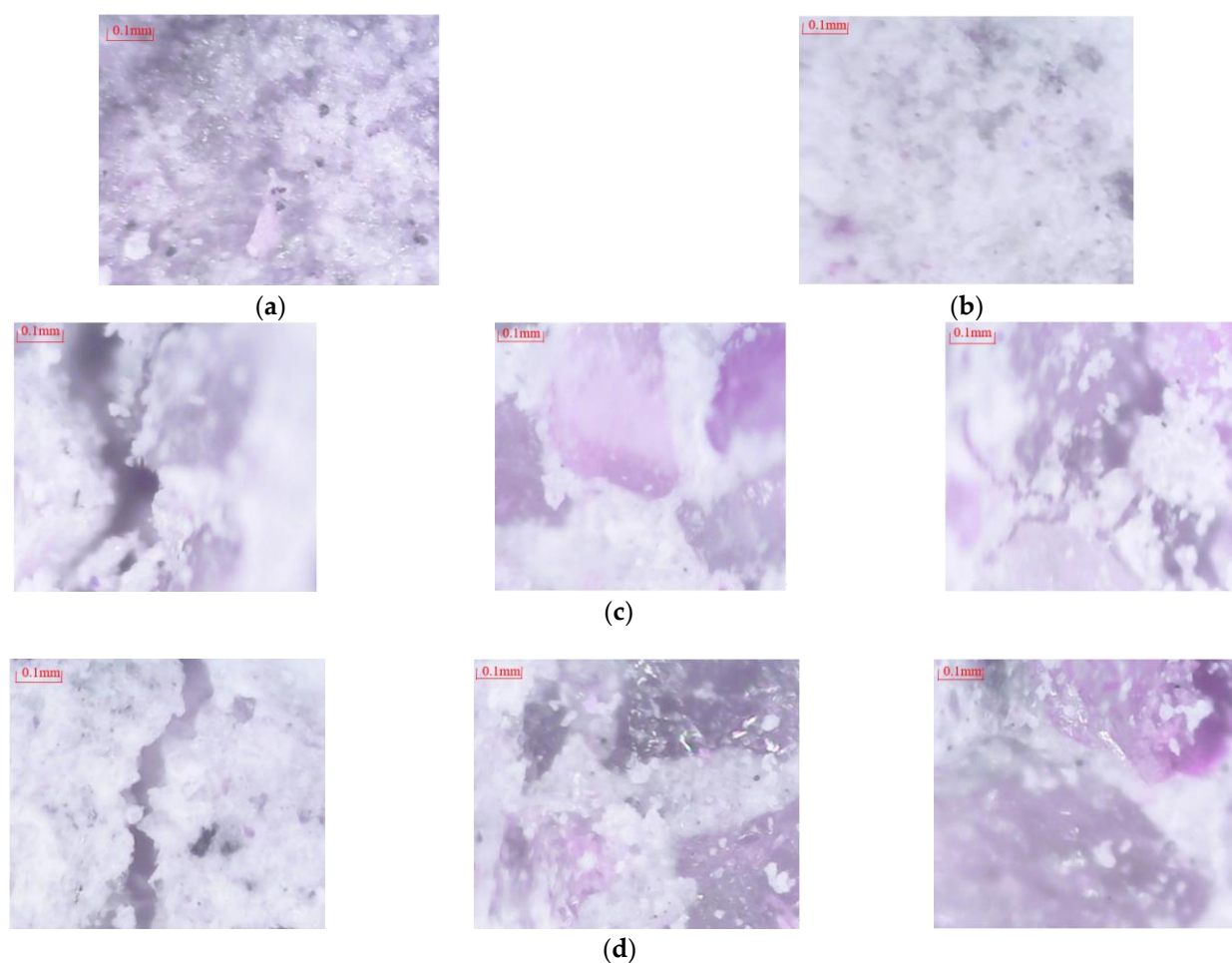
**Figure 10.** Microscopic fracture morphology of similar materials. (**a**) Microscopic view of the surface of a mudstone-like specimen. (**b**) Surface micro-view map of a sandstone-like specimen. (**c**) Mesoscopic fracture morphology of mudstone-like specimens. (**d**) Micro-fracture morphology of sandstone-like specimens.

A comparison of Figure 10a,b shows that mudstone and sandstone are similar materials. Although they are all mixed with water, cement, and sand, the ratios are different, and the microstructures of similar materials are also different. Sandstone−like materials show more holes and micro-cracks and a lower density than mudstone-like materials. For mudstone-like materials, as these consist of more sand particles than cement, cement hydration reaction products fill the space between sand particles and bond these together. However, because of excessive sand components, hydration products are not densely filling all voids. As shown in Figure 10c, although there is filling material between sand particles, the voids are not densely filled and holes remain. However, the amount and diversity of sand particles has increased, and a subset of particles has a suitable shape. Their surface is smooth, and therefore, hydration products cannot easily adhere to their surface, thus forming a wrapping. Once subjected to impact load, this wrapping effect causes the dynamic response frequency of the hydration products and sand particles to the shock wave to differ, and different frequencies will be generated. The resulting self-vibration causes the destruction of the structure, thus exposing the wrapped sand. Affected by the lack of compactness of the filling material, the destruction of mudstone-like materials mostly happens between sand grains. As shown in Figure 10d, the cement hydration product of sandstone-like materials better and more densely fills the sand gaps. The fracture shape of the impact sample has a similar structure to mudstone, both of which are damaged from the sand−grain contact surface. However, the damage of the sandstone-like material is mainly

caused by the destruction of particles and hydration products. The crack direction may either pass through the hydration products or run along the sand grains. Especially with increasing cement content and decreasing sand content, a considerable amount of hydration products will form, which can firmly bond together thus reducing the appearance of pores and micro-cracks.

## 4. Dynamic Splitting Mechanical Properties of Similar Materials

Rock is a medium with much lower tensile strength than compressive strength. Under dynamic action, in addition to impact compression, the rock mass will also be affected by reflection stretch on the surface and side of the specimen. The tensile strength is designed to break rock. One of the important factors considered is that the determination of the dynamic tensile strength of the rock is the same as the static tensile strength, and the split test is the main method. Figure 11 shows the stress–strain curves of sandstone-like materials and mudstone-like materials in the impact splitting process. The basic dimensions of the specimen and the results of the average strain rate, dynamic splitting strength, and wave velocity under 0.2 MPa impact pressure are shown in Table 5.
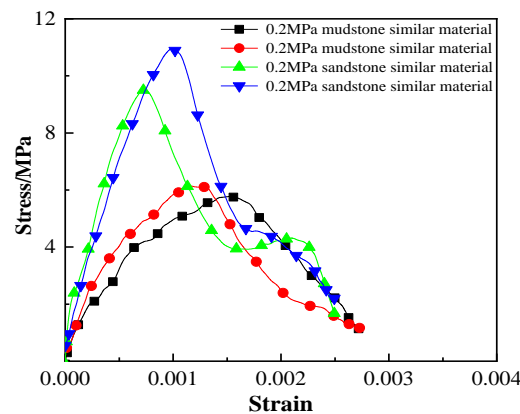


**Figure 11.** Splitting stress–strain curves of specimens under different impact pressures.

**Table 5.** Results of dynamic splitting experiments for similar materials.

| Specimen Type | Test Block Number | Impact Air Pressure (MPa) | Specimen Size (Average Value) | | Wave Speed (m/s) | Average Strain Rate(s$^{-1}$) | Peak Stress (MPa) | Ultimate Strain $\varepsilon$ |
| | | | Diameter (mm) | Height (mm) | | | | |
|---|---|---|---|---|---|---|---|---|
| Mudstone similar material | 2 | | 49.12 | 25.78 | 2950 | 114 | 5.75 | 0.0027 |
| | 9 | 0.2 | 49.17 | 24.14 | 2960 | 115 | 6.11 | 0.0027 |
| Sandstone similar material | 1 | | 49.35 | 26.68 | 3521 | 107 | 9.59 | 0.0025 |
| | 16 | | 49.54 | 26.24 | 3583 | 108 | 10.89 | 0.0025 |

Note: Considering the discrete type of impact test, two relatively close test data sets were selected for each group.

The data in Figure 11 show that in the initial stage, the dynamic stress–strain relationship of similar materials increases linearly with increasing strain, then reaches the peak of tensile strength, after which the stress decreases instantaneously and the specimen is damaged. The results of dynamic splitting of mudstone-like and sandstone-like materials are similar and the peak splitting strains of both materials are also similar; however, the dynamic tensile strength of sandstone-like materials is higher. The dynamic tensile strength of the specimen is a quarter of the dynamic compressive strength under the same air pressure. Under the action of dynamic load, the tensile–compression ratio of the material increases.

Figure 12 shows that impact fracturing and fracture state of mudstone-like materials is conventional, with the main crack failure in the middle, but with excessive smashing locally. The impact process of sandstone-like materials not only produces cracks along the

middle, but also near the main crack. Secondary cracks run parallel to the main crack, and bending cracks are also observed. The damage shape is more complicated than that of mudstone-like materials. Considering the cause of damage, the main reason is the reflection of stress waves. Sandstone-like materials have higher strength. When the stress–strain curve of Figure 12 reaches the peak of tensile strength, the strain value of sandstone-like materials is relatively small; however, the stress of sandstone-like materials decays rapidly in the later stage, and a plateau appears during the attenuation process. When an external load is applied, only the energy stored during internal splitting of the rock is released to supplement stress attenuation. Therefore, at this stage, the stress waves of the upper and lower parts of the main crack in the rock mass appear unloaded, and secondary cracks emerge along the main crack.

(**a**)

(**b**)
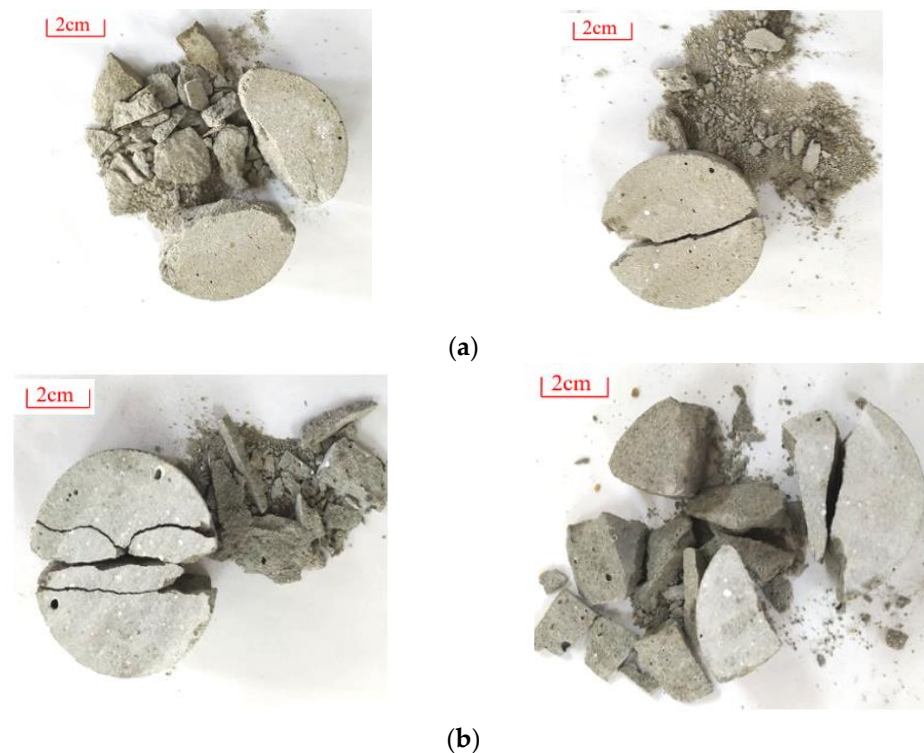
**Figure 12.** Fracture failure modes of specimens under different impact pressures. (**a**) Impact crushing form of mudstone-like material (0.2 MPa crushing form), (**b**) impact crushing form of sandstone-like material (0.2 MPa crushing form).

## 5. Dynamic Compression Mechanical Properties of Similar Materials under Active Confining Pressure

The setup used for the dynamic compression impact mechanics test of rock-like materials under active confining pressure is shown in Figure 13. The device is loaded by oil pressure, and the active confining pressure is applied through the manual booster pump. The liquid transmits the pressure to the sealing ring of the wrapped test piece. The sealing ring transmits the pressure to the circumferential direction of the test piece, and the sealing ring can be pressurized. The liquid pressure of the pressurizing device can be flexibly adjusted to adjust the active confining pressure loading. The sealing ring is made of nitrile rubber. During the test, the incident pressure bar was first inserted into the confining pressure loading device, then the test piece was placed in the middle of the confining pressure loading device. Then, the transmission rod was inserted to ensure that the incident rod, the test piece and the transmission rod were in close contact, and then the oil pressure load was applied to the set value for impact.
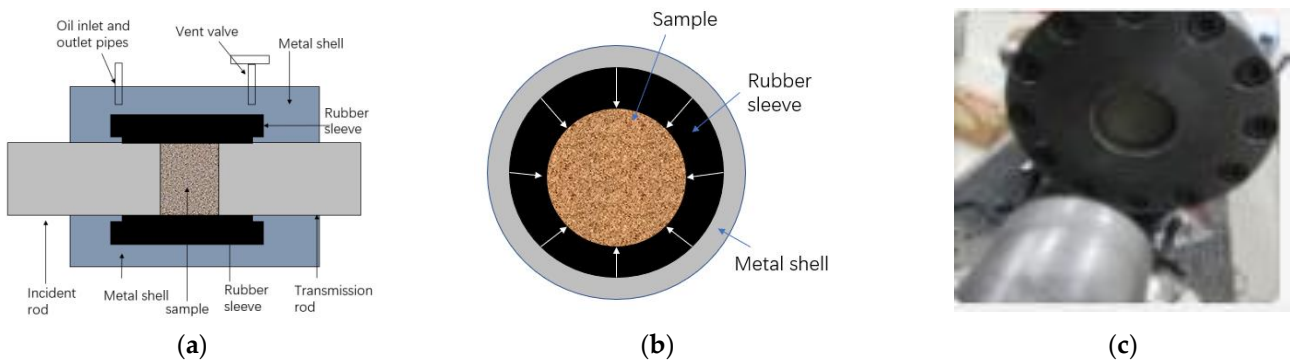
**Figure 13.** Uniaxial impact compression test under active confining pressure. (**a**) Active confining pressure diagram, (**b**) stress diagram of sample, (**c**) confining pressure loading device.

According to rock properties and confining pressure loading conditions, confining pressure is mainly applied during the test to explore the dynamic compression characteristics and fracture of the material under confining pressure.

For an impact air pressure of 0.4 MPa, the dynamic stress–strain curves of mudstone-like materials under different confining pressures are shown in Figure 14. The stress–strain curves of sandstone-like materials are shown in Figure 15.
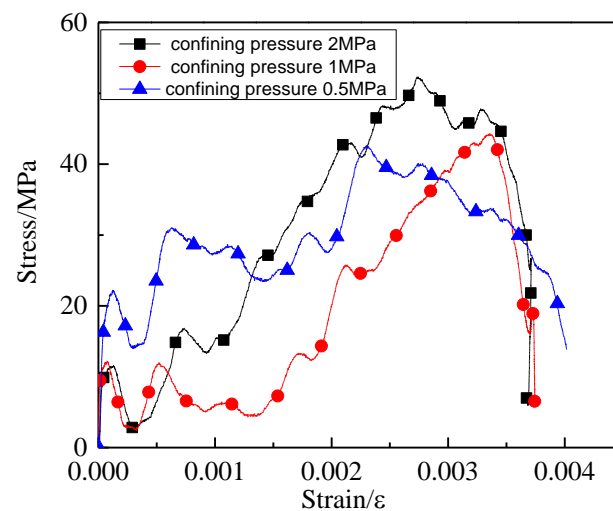


**Figure 14.** Dynamic stress–strain curve of mudstone-like material under active confining pressure.
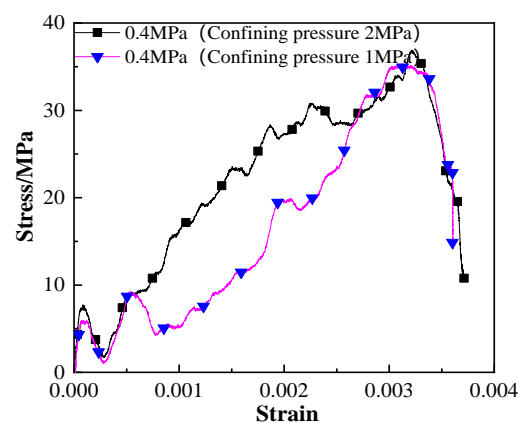


**Figure 15.** Dynamic stress–strain curve of active confining pressure of sandstone-like material.

The data in Figure 14 show that under the same impact load, the dynamic peak strength of mudstone increases with increasing confining pressure on the specimen. However, the growth coefficient of the peak dynamic strength of the rock is small because of the influence of the confining pressure loading strength. Compared with the non-confining pressure, the stress and strain of the specimens shows a clear increase in the elastic growth stage, when the failure is faster, and dynamic strength increases. The dynamic strength peaks of the specimens under the action of 0.5, 1, and 2 MPa increase. The main reason for this is that the lateral displacement of the specimen is constrained under the action of confining pressure. Under the action of stress wave, both axial splitting and tensile failure should occur. The squeeze offsets part of the tensile stress, so that the rock is still in a complete state.

Figure 15 shows that under the same impact load, the dynamic peak strength and peak strain of sandstone-like materials exert little effect with increasing confining pressure of the specimen. However, as the stress–strain curve of the specimen changes, the loading process becomes elastic. The stage is reduced and then rises. Compared with the lack of confining pressure, the dynamic strength is reduced. The peak dynamic strength of the specimen under the action of confining pressures of 1 and 2 MPa is reduced to half of that of no confining pressure. This result conflicts with the result of mudstone-like materials with increasing strength as the confining pressure increases. In response to no confining pressure impact, the sample strain peaks are similar, but the average strain rate changed from 139–156 $s^{-1}$ without confining pressure to 178 $s^{-1}$ at 0.5 MPa confining pressure, and 190 $s^{-1}$ at 1 MPa confining pressure. At 213 $s^{-1}$ under confining pressures of 1 or 2 MPa, when the specimen satisfies the stress balance, the average strain rate is closely related to the reflected wave from the mudstone-like material. The increase in the strain rate indicates that the peak of the reflected wave increases. The pressure is roughly equal, i.e., the average strain rate integral is the same, indicating that under the condition of a specific impact reflection energy, confining pressure loading causes an increase in the peak value of the reflected stress wave. Both with and without confining pressure, the average strain rate of sandstone-like materials changed from 139–156 $s^{-1}$ without confining pressure to 180 $s^{-1}$ under 1 MPa confining pressure, and 184 $s^{-1}$ under 2 MPa confining pressure. The strain peak value changed from 0.0019–0.0020 to 0.0036, indicating that the impact reflection energy of sandstone-like materials increased. According to the one-dimensional stress wave propagation law, under the same time action, the reflection energy increases, i.e., the reflection coefficient increases. The material wave impedance is related. The larger the material wave impedance value, the smaller the reflection coefficient, and vice versa. This means that the wave impedance value of sandstone-like materials becomes smaller under the action of confining pressure. The wave impedance is the product of the material density and the wave velocity. Under the action, the density of the material generally does not change significantly. From this analysis, under the action of no confining pressure, the peak axial strain of the sandstone-like material is very small, and the specimen is damaged; however, under the action of confining pressure, the axial deformation of sandstone increased greatly, but the sample is not completely destroyed. Because of the increasing axial deformation, the internal damage of the material increases. Under constant density, the wave speed decreases, which causes an increase in reflected stress waves and strain rate of sandstone-like materials. As the strain rate increases, the strength decreases. The active confining pressure loading conditions and test impact data results of rock-like materials are shown in Table 6.

The data in Table 6 on the active confining pressure impact test data of similar rock materials show that when the impact load is low, under an impact pressure of 0.2–0.3 MPa, the differences between stress, strain, and average strain rate of mudstone-like materials under the action of confining pressure are small. There is a decreasing tendency compared with no confining pressure, and the reason is consistent with the above analysis. This also shows that the confining pressure affects the dynamic strength of the material significantly beyond a certain range. In this test, if the impact load exceeds 0.4 MPa, the effect is manifested. Under the action of low confining pressure, the dynamic strength loss of the

test piece is more severe for the rock-like material, the stress value is reduced by 1/4, but the strain peak value increased significantly. The failure mode of the test piece under the action of active confining pressure is shown in Figure 16.

**Table 6.** Experimental results of active confining pressure impact of sandstone-like materials.

| Material | Serial Number | Impact Air Pressure (MPa) | Active Confining Pressure (MPa) | Specimen Size (Average Value) | | Average Strain Rate (s⁻¹) | Peak Stress (MPa) | Peak Strain ε |
|---|---|---|---|---|---|---|---|---|
| | | | | Diameter (mm) | Height (mm) | | | |
| Mudstone-like material | 10 | 0.2 | 0.5 | 48.95 | 25.95 | 88 | 17.39 | 0.0018 |
| | 22 | 0.2 | 1 | 49.01 | 25.64 | 85 | 17.14 | 0.0021 |
| | 24 | 0.2 | 2 | 48.90 | 26.89 | 90 | 17.32 | 0.0024 |
| | 26 | 0.3 | 0.5 | 48.85 | 25.91 | 139 | 27.00 | 0.0032 |
| | 20 | 0.3 | 1 | 48.75 | 26.02 | 145 | 29.34 | 0.0027 |
| | 14 | 0.3 | 2 | 48.80 | 24.86 | 156 | 25.96 | 0.0028 |
| | 15 | 0.4 | 0.5 | 49.45 | 25.58 | 178 | 42.49 | 0.0037 |
| | 19 | 0.4 | 1 | 48.80 | 23.24 | 190 | 49.71 | 0.0037 |
| | 18 | 0.4 | 2 | 48.46 | 25.32 | 213 | 51.38 | 0.0037 |
| Sandstone-like material | 7 | 0.2 | 1 | 49.33 | 24.84 | 83 | 11 | 0.0017 |
| | 6 | 0.2 | 2 | 49.47 | 25.08 | 89 | 12 | 0.0019 |
| | 11 | 0.3 | 1 | 49.31 | 25.71 | 151 | 18 | 0.0030 |
| | 14 | 0.3 | 2 | 49.30 | 25.41 | 150 | 22 | 0.0031 |
| | 17 | 0.4 | 1 | 49.22 | 24.45 | 180 | 35 | 0.0036 |
| | 20 | 0.4 | 2 | 49.27 | 25.46 | 184 | 36 | 0.0036 |

Note: Considering the discrete type of impact test, two to three relatively close test data sets were selected for each group.



(a) 2 MPa confining pressure 0.2 impact (b) 2 MPa confining pressure 0.3 impact (c) 2 MPa confining pressure 0.4 impact

(**1**)
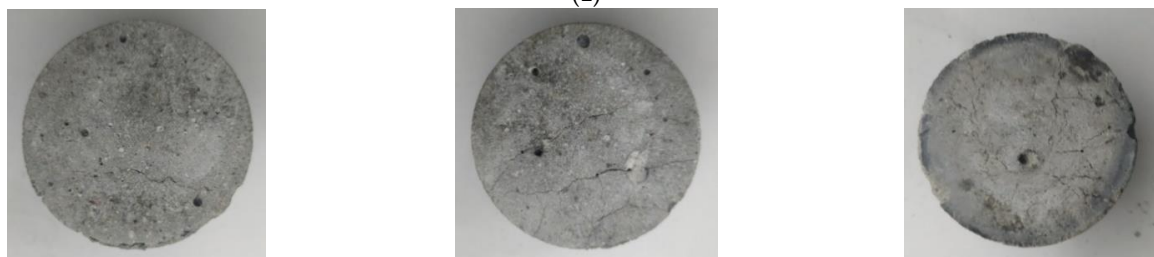


(a) 2 MPa confining pressure 0.2 impact (b) 2 MPa confining pressure 0.3 impact (c) 2 MPa confining pressure 0.4 impact

(**2**)

**Figure 16.** Failure modes of specimens under active confining pressure. (**1**) Similar material failure form of active confining mudstone, (**2**) similar material failure mode of active confining sandstone.

Figure 16 shows that under the action of active confining pressure, the specimen is not apparently damaged when the active confining pressure of mudstone-like materials is impacted by low air pressure. As this pressure increases. It shows peripheral spalling failure, that is, the test piece spalls layer by layer from the edge to the inside of the test piece. The internal layer of the specimen is peeled off, and the sandstone-like material is

similar to the material in the active confining pressure failure form. Under the action of low air pressure, the specimen cracks axially. With increasing impact pressure, the internal damage of the specimen gradually becomes severe, and cracks emerge on the surface. The occurrence of cracks indicates axial splitting and tensile cracking, which is related to the radial expansion of the specimen when subjected to axial compression. This is also related to the previous reasoning where sandstone-like material is subject to low confining pressure. The strength is low, but the reason for the higher strain rate is the same, i.e., the damage in the axial direction is generated inside the specimen, and as the damage develops further, axial cracks emerge, and the wave speed of the specimen is reduced.

## 6. Discussion

Through the dynamic impact tests, the mechanical properties of mudstone-like and sandstone-like materials under dynamic load were explored. Because of the influence of diagenesis, the internal structure of deep coal mine rocks is complex and changeable, and because of the special geographical environment of these deep rocks, they can be taken out completely. By adjusting the proportion of mudstone-like and sandstone-like materials, a pouring model of these materials is matched with a key research property of the original rock. This achieved replacement of deep rock samples with similar materials. Then, the rules of key properties of this kind of material can be more comprehensively studied under different external load environments. This study carried out relevant experiments, analyzed and obtained relevant conclusions, but the research results were based on the experimental data. In nature, the state of rock is very complex, it does not consider the role of effective stresses, which, mainly in the case of mining activities (e.g., blasts), can be associated with highly heterogeneous and time-varying pore pressure fields (associated with liquids or gases present in the porous medium). The role of heterogeneous fluid pressure fields in rock fracturing is not yet well understood and, on this issue, there are still many open issues. This paper provides experimental results in dry conditions, nevertheless, it is not sufficient to translate these results in terms of effective stress and apply them to the case of fluid filled materials. This is explained in detail by Guerriero and Mazzoli (2021) [19]. New test methods such as high-speed cameras and DIC can be used during the test. Poisson's ratio can be obtained by employing DIC, which can also be used for full field strain validation with the FEA.

## 7. Conclusions

This paper focused on mudstone and sandstone rocks of a typical deep roadway. Similar materials were prepared, using the 50 mm diameter separated Hopkinson test device and dynamic impact tests of mudstone, sandstone, and similar materials were carried out under different impact pressures. The main components and microstructures of the rock samples were combined. The following conclusions can be drawn:

(1) Mudstone has low mechanical strength and poor physical performance indicators. Under impact load, circumferential fracture failure and axial splitting tensile failure occur. Sandstone shows axial splitting tensile failure and crushing failure. Mudstone and sandstone are broken with increasing impact air pressure. Within the tested strain rate range, the dynamic uniaxial compressive strengths of mudstone and sandstone increase exponentially with increasing strain rate, showing a strong strain rate effect.

(2) Mudstone has low strength and low wave impedance, and the initial reflection stress at the incident end of the specimen is large. Under the combined action of reflection stress and transmission stress, mudstone specimens preferentially produce circular cracks, which slow the propagation of reflected and transmitted stress waves in the specimen. This can cause the specimen to reach a stress balance at about 150 μs. In the equilibrium state, the effect of stress wave penetration and reflection causes the rapid generation of axial cracks in the specimen, which propagate and eventually fail. The breaking resistance value of sandstone exceeds that of mudstone. Under the combined action of the reflected

wave and transmitted wave, the strength growth is higher than that of mudstone, and the specimen reaches stress balance sooner than the mudstone specimen.

(3) The absorption energy, transmission energy, and reflection energy of mudstone specimens increase with increasing incident energy. These increases follow linear, logarithmic, and quadratic functions, respectively. The absorption energy of specimens can be measured by the energy consumption density per unit volume, energy consumption per unit mass, and absorption impedance ratio energy characterization. All three increase linearly with increasing incident energy and with the strain rate in a quadratic function.

(4) With increasing impact pressure, the average strain rate, dynamic strength, and peak strain of mudstone and sandstone-like materials all increase. The dynamic strengths of both mudstone and sandstone-like materials follow a trend of power function increase in dynamic strength with increasing strain rate. The regularity of the original rock is consistent.

(5) The dynamic splitting stress–strain curves of mudstone-like and sandstone-like materials are similar, but the dynamic tensile strength of sandstone-like materials is higher. Mudstone-like materials are mainly cracked in the middle, where excessive crushing can also be observed. Sandstone shows a similar impact process except cracks appear in the middle. Because of the unloading effect, secondary cracks are also generated near the main cracks.

(6) As the active confining pressure increases, the dynamic strength peak growth coefficient of mudstone-like materials is small. Compared with no confining pressure, the elastic growth stage of mudstone increases significantly, and the damage is faster. This is similar to sandstone without confining pressure. The peak value of the dynamic strain of the material increases, the axial deformation increases, the internal damage of the material increases, and the longitudinal wave velocity decreases. This causes an increase in the reflected stress wave.

**Author Contributions:** Validation, M.W., P.G. and Q.Z.; formal analysis, Q.Z.; investigation, X.L.; resources, P.G.; data curation, M.W.; writing—original draft preparation, P.G.; writing—review and editing, M.W. All authors have read and agreed to the published version of the manuscript.

**Data Availability Statement:** The data used to support the findings of this study are included within the article.

**Conflicts of Interest:** The authors declare no conflict of interest.

# References

1. Li, Q.; Li, S. Experimental study on rock mechanical properties of ultra deep sandstone reservoir. *J. Rock Mech. Eng.* **2021**, *40*, 948–957.
2. Zhao, Y. Some reviews of the development of rock mass mechanics and some unsolved hundred year problems. *J. Rock Mech. Eng.* **2021**, *40*, 1297–1336.
3. Xie, H.; Gao, F.; Ju, Y.; Zhang, R.; Gao, M.; Deng, J. Several disruptive technological ideas and research directions in the field of deep earth science. *Eng. Sci. Technol.* **2017**, *49*, 1–8.
4. Zhang, Z.; Xie, H.; Zhang, R.; Zhang, Z.; Gao, M.; Jia, Z.; Xie, J. Deformation damage and energy evolution characteristics of coal at different depths. *Rock Mech. Rock Eng.* **2019**, *52*, 1491–1503. [CrossRef]
5. Yuan, L.; Zhang, N.; Kan, J.; Wang, Y. Concept, model and forecast of green coal resources in China. *J. China Univ. Min. Technol.* **2018**, *47*, 1–8.
6. Feng, X.; Xiao, Y. Study on the incubation process of rockburst. *Chin. J. Rock Mech. Eng.* **2019**, *38*, 649–673.
7. Bai, Y. *Rock Blasting Damage Model and Its Numerical Experiment under the Influence of In-Situ Stress*; Northeastern University: Shenyang, China, 2014.
8. Xie, H. Research progress on deep rock mass mechanics and mining theory. *J. China Coal Soc.* **2019**, *44*, 1283–1305.

9.  Wang, M.; Wang, H.; Zong, Q. Experimental study on energy dissipation of coal mine mudstone under impact load. *J. Coal* **2019**, *44*, 1716–1725.
10. Wang, M.; Wang, H.; Zong, Q. Analysis of impact dynamic mechanical characteristics and fracture characteristics of mudstone in coal mine. *Vib. Impact* **2019**, *38*, 137–143.
11. Zhao, G.; Ma, W.; Meng, X. Failure mode and energy characteristics of rock materials under dynamic load. *Rock Soil. Mech.* **2015**, *36*, 3598–3605, 3624. [CrossRef]
12. Li, X.; Gong, F. Research progress and prospect of deep mining rock mechanics based on coupled static-dynamic loading testing. *J. Coal* **2021**, *46*, 846–866. [CrossRef]
13. Li, X. Study on fracture and crushing mechanism of rock materials under strong impact load. *J. Rock Mech. Eng.* **2021**, *40*, 432.
14. Zhou, Y.; Sheng, Q.; Li, N.; Fu, X. Study on dynamic enhancement factor model of stren gth and modulus of rock materials under different strain rates. *J. Rock Mech. Eng.* **2020**, *39*, 3245–3259.
15. Liu, S. Catastrophe model and chaotic mechanism of combined coal rock failure and instability under dynamic and static loading. *J. Coal* **2014**, *39*, 292–300.
16. Li, X.; Xu, Q.; Xie, H.; Xiao, M.; He, J. Damage constitutive and evolution characteristics of fractured rock under static and dynamic load coupling. *J. Rock Mech. Eng.* **2015**, *34*, 3029–3036.
17. Peng, L.; Hu, X.; Su, G.; Qin, Z.; Lu, H.; He, B. Cracking characteristics of the surrounding rocks of a hydraulic tunnel under high geothermal conditions: A model test. *Rock Mech. Rock Eng.* **2021**, *54*, 1369–1390. [CrossRef]
18. Fu, H.; Qi, S.; Shi, Z.; Zeng, L. Mixing ratios and cementing mechanism of similar silty mudstone materials formodel tests. *Adv. Civil Eng.* **2021**, *2021*, 2426130. [CrossRef]
19. Vincenzo, G.; Stefano, M. Theory of Effective Stress in Soil and Rock and Implications for Fracturing Processes: A Review. Geosciences. *Geosciences* **2021**, *11*, 119.